International Journal of Modern Physics C
Vol. 18, No. 4 (2007) 661–666

World Scientific
www.worldscientific.com

SIMULATING TIME HARMONIC FLOWS WITH THE REGULARIZED L-BGK METHOD

LILIT AXNER*,‡, JONAS LATT†, ALFONS G. HOEKSTRA*, BASTIEN CHOPARD† and PETER M. A. SLOOT*

*Section Computational Science, University of Amsterdam
Kruislaan 403, 1098 SJ Amsterdam, The Netherlands

†Computer Science Department, University of Geneva
CH-1211 Geneva 4, Switzerland

‡labraham@science.uva.nl

A recent improvement of the lattice BGK model, based on a regularization of the pre-collision distribution function, is applied to three dimensional Womersley flow. The accuracy and the stability of the model are essentially improved by using this regularization. A good agreement with analytical Womersley solution is presented, as well as an improvement of the accuracy over standard L-BGK. Numerical stability of the scheme for a range of Reynolds and Womersley numbers is also presented, demonstrating an enhancement of the stability range of L-BGK for this type of flows.

Keywords: Regularized L-BGK model; Time-harmonic flow; accuracy; numerical stability.

PACS Nos.: 11.25.Hf, 123.1K.

1. Introduction

The lattice Boltzmann BGK method (L-BGK)[1,2,3] has been actively applied for simulation of fluid flows in many CFD applications, see e.g. Ref. 4, 5, 6, 7, 8, 9. However, it is known that L-BGK suffers from numerical instabilities at high Reynolds numbers (Re). Several solutions have been proposed to improve the method in this respect[10,11]. In this paper we follow another route, we choose to use the regularization scheme proposed by Latt and Chopard[12]. In this RL-BGK scheme, the simulated kinetic variables are submitted to a small correction (the regularization), after which they only depend on the local density, velocity, and momentum flux. This correction is immediately followed by the usual L-BGK collision term. The effect of the regularization step is to eliminate non-hydrodynamic terms, known as "ghost variables", and to enforce a closer relationship between the discrete, kinetic dynamics and the macroscopic Navier-Stokes equation.

‡Corresponding author.

We study the performance of the RL-BGK through a numerical simulation of the time-harmonic Womersley[13] flow for 3D geometries. Further, we analyze the accuracy of the scheme by comparison of the simulation results with analytical Womersley solution. We also present stability analysis of the model for the benchmark flows.

2. Regularized lattice Boltzmann model

In the L-BGK method, the dynamics of the discrete distribution function f_i is described by means of a relaxation to a local equilibrium term:

$$f_i(\vec{x}+\vec{c}_i,t+1)-f_i(\vec{x},t)=-\omega\left(f_i(\vec{x},t)-f_i^{(eq)}(\rho(\vec{x},t),\vec{u}(\vec{x},t))\right), \tag{1}$$

where the relaxation parameter ω is related to the local fluid viscosity, here $\vec{c}_i$ is a discrete set of velocities. The evolution of the f's, as described by Eq. 1 depends only on the macroscopic particle density (ρ) and fluid velocity ($\vec{u}$), and the off-equilibrium values of the distribution functions, $f_i^{(neq)}=f_i-f_i^{(eq)}$. This becomes clear when the dynamics is cast into the following form:

$$f_i(\vec{x}+\vec{c}_i,t+1)=(1-\omega)f_i^{(neq)}(\vec{x},t)+f_i^{eq}(\rho(\vec{x},t),\vec{u}(\vec{x},t)). \tag{2}$$

It is well known that Eq. 1 can be related to the Navier-Stokes equation for a fluid through a multi-scale, Chapman-Enskog expansion of the f_i's. This procedure uses an approximation of the off-equilibrium term as $f_i^{(neq)}\approx f_i^{(1)}$, where

$$f_i^{(1)}=-\frac{t_i}{\omega c_s^2}Q_{i\alpha\beta}\partial_\alpha\rho u_\beta, \tag{3}$$

In this expression, we have introduced the symmetric stress tensor $Q_{i\alpha\beta}=c_{i\alpha}c_{i\beta}-c_s^2\delta_{\alpha\beta}$, defined in terms of the Kronecker symbol $\delta_{\alpha\beta}$. Here t_i is the weight factor of corresponding lattice directions. Under the same approximation, the stress tensor $\Pi_{\alpha\beta}^{(neq)}=\sum_i f_i^{(neq)}c_{i\alpha}c_{i\beta}$ can be related to the velocity gradients as follows:

$$\Pi_{\alpha\beta}^{(neq)}\approx\Pi_{\alpha\beta}^{(1)}=-c_s^2/\omega(\partial_\alpha(\rho u_\beta)+\partial_\beta(\rho u_\alpha)). \tag{4}$$

The key idea of the regularized BGK model is to exploit the symmetries both of Q and $\Pi^{(neq)}$ to express $f_i^{(neq)}$ fully in terms of the stress tensor. Indeed, by using the symmetry $Q_{i\alpha\beta}=Q_{i\beta\alpha}$ Eqs. 3 and 4 can be combined to obtain

$$f_i^{(1)}=\frac{t_i}{2c_s^4}Q_{i\alpha\beta}\Pi_{\alpha\beta}^{(neq)}. \tag{5}$$

This concludes the derivation of the regularized BGK model. In this new model, the term $f_i^{(neq)}$ is replaced by $f_i^{(1)}$, and Eq. 2 becomes:

$$f_i(\vec{x}+\vec{c}_i,t+1)=(1-\omega)f_i^{(1)}(\Pi(\vec{x},t))+f_i^{eq}(\rho(\vec{x},t),\vec{u}(\vec{x},t)). \tag{6}$$

All the macroscopic variables, Π, $\vec{u}$ and ρ, are computed locally from the particle distribution functions f_i. All the terms contained in Eq. 6 can be written out properly so as to obtain a numerical model just as efficient as the original L-BGK.

More details on the regularized LB model, and a discussion of its relation to Multiple relaxation time (MRT) models, can be found in Ref. 12.

We compare the velocity profiles of the simulated flow with the analytical Womersley solution[13]. For the accuracy measurements we define a simulation error ($\widetilde{Er}$) as

$$\widetilde{Er} = \frac{1}{T}\sum_{t}\frac{\sum_x |\boldsymbol{u}_{th}(\boldsymbol{x},t) - \boldsymbol{u}_{lb}(\boldsymbol{x},t)|}{\sum_x |\boldsymbol{u}_{th}(\boldsymbol{x},t)|}, \tag{7}$$

where $\boldsymbol{u}_{th}(t)$ is the analytical Womersley solution[13], $\boldsymbol{u}_{lb}(t)$ is the simulated velocity, and T is the number of time steps per period. Here

$$\boldsymbol{u}_{th} = \frac{AR^2}{\nu}\frac{1}{i^3\alpha^2}\left\{1 - \frac{J_0\left(\alpha i^{3/2}x\right)}{J_0\left(\alpha i^{3/2}\right)}\right\}e^{i\omega t}, \tag{8}$$

where R is the radius of the tube, x is defined as $x = r/R$, $\omega = \frac{2\pi}{T}$ is the circle frequency, $Ae^{i\omega t}$ is the pressure gradient driving the flow, i stands for imaginary unit, J_0 is the zero order Bessel function and α is the Womersley number

$$\alpha = \frac{D}{2}\sqrt{\frac{\omega}{\nu}}. \tag{9}$$

with D diameter and ν viscosity. In the next section we show the obtained experimental results and accuracy measurements.

3. Accuracy and Stability of RL-BGK

We use the three dimensional 19-velocity (D3Q19) model[14] for time harmonic flows[15]. The fluid flow is quasi-incompressible in a straight tube with rigid walls. On the walls we use Bouzidi boundary conditions (BBC)[16] and bounce back on the links(BBL). The test case presented here is a $36 \times 38 \times 38$ tube with body force driven flow and periodic inlet/outlet boundary conditions. We studied multiple test-cases with a range of Reynolds (Re) and Womersley (α) numbers. We compared the velocity profiles for every $0.1 \times T$ time-step with analytical Womersley solutions and measured the $\widetilde{Er}$ according to Eq. 7. In Fig. 1 we show the comparison of the velocity profiles for $Re = 300$, $\alpha = 16$ and $u_{max} = 0.1$ (i.e. Mach number $Ma = 0.2$) velocity case. From Fig. 1 we see that the agreement for the RL-BGK scheme (right) is better in comparison with L-BGK (left). From our simulations we observe that in case of BBC the improvement of accuracy is not as pronounced as in case of BBL. For L-BGK in case of BBL the error $\widetilde{Er} = 9 \times 10^{-3}$ while for RL-BGK $\widetilde{Er} = 3.2 \times 10^{-3}$. Table 1 lists $\widetilde{Er}$ for a range of Re and α for both RL-BGK and L-BGK[20].

From Table 1 we can see that in case of BBL $\widetilde{Er}$ is approximately three times smaller for the RL-BGK scheme. Thus, if we use the RL-BGK scheme aiming at the same accuracy as L-BGK, the execution time will be lower by a factor of $1.7^3 \approx 5$. From our measurement we observe that the execution time of RL-BGK in comparison with L-BGK is larger by $\approx 3\%$ - 4%.

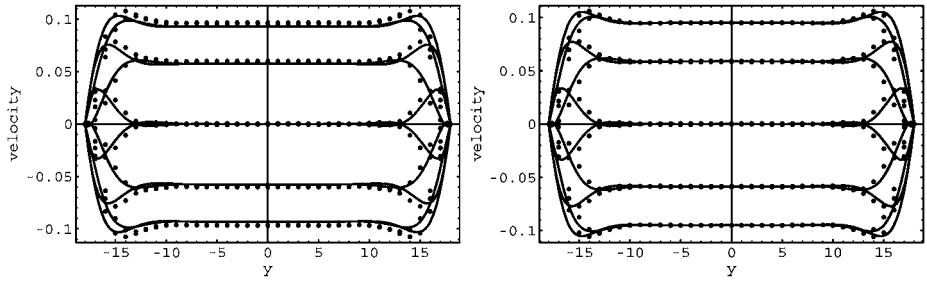

Fig. 1. Comparison of velocity profiles of simulated (dots) L-BGK (left) and RL-BGK (right) schemes with analytical Womersley (solid lines) solutions for flow in the tube with diameter $D = 36$, $\alpha = 16$ and $Re = 300$.

Table 1. Simulation error $\widetilde{Er}$ for a range of Re and α.

Re	50	100	600	1200	3050
		RL-BGK			
$\alpha = 6$	0.003	0.004	0.005	0.02	0.05
$\alpha = 10$	0.003	0.003	0.005	0.01	0.03
$\alpha = 16$	0.002	0.003	0.004	0.01	0.02
		L-BGK			
$\alpha = 6$	0.01	0.01	0.02	0.06	0.2
$\alpha = 10$	0.008	0.009	0.01	0.03	0.1
$\alpha = 16$	0.007	0.009	0.01	0.03	0.07

3.1. *Numerical stability*

Numerical stability of the L-BGK has been an issue for many authors[17,18,19,20]. We measured the numerical stability of RL-BGK scheme. In these measurements we fix Ma for $u = 0.1$, and we push Re to its highest possible value for a range of α. For a 3D tube we fix the diameter to $D = 36$ lattice points[20]. We applied two different boundary conditions: Bounce back on links (BBL) and BBC boundary conditions on the walls. We also performed the same stability measurements on a real geometry, a human abdominal aorta with $D_{max} = 18$, and BBL on walls for time harmonic flow[15]. We consider the simulation to be unstable when the total momentum in the system diverges[20].

In Fig. 2 we compared the stability limits of L-BGK with RL-BGK for the same simulation parameters. As we can see from Fig. 2 the regularized method is more stable than L-BGK. In case of the tube with BBC boundary conditions the improvement is not as obvious as in case of BBL. With the use of BBL boundaries, RL-BGK simulations could reach a Reynolds number five times higher than L-BGK on a stationary flow, and two times higher on time-harmonic flows. For abdominal aorta the improvement is from three to four times.

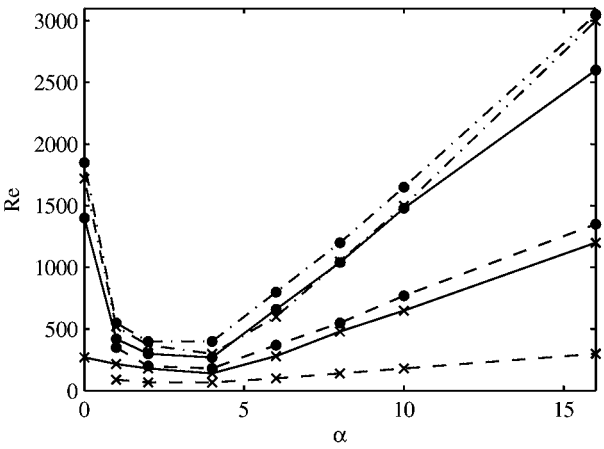

Fig. 2. Comparison of the threshold values of Reynolds number for RL-BGK(-•-)and L-BGK (-x-) schemes for simple tube with $D = 36$ for BBC ($-\cdot-\cdot-$) and for BBL(_ _), and abdominal aorta with $D_{max} = 18$ for BBL(−−). The range of Womersley number is from 1 to 16 for $u_{max} = 0.1$.

4. Conclusion

We have presented numerical simulation results of time harmonic Womersley flow in a 3D tube by applying the regularized L-BGK scheme. We compared the velocity profiles from simulations with the analytical Womersley solution. We showed that the accuracy associated with RL-BGK is essentially higher than with L-BGK by comparing the simulation errors. This implies that if we use the RL-BGK scheme with the same accuracy as L-BGK the execution time will decrease significantly[20]. We also presented the stability measurements for the RL-BGK scheme where we reached higher Reynolds numbers than in case of the L-BGK scheme. For a 3D time-harmonic flow we achieved three to five times higher Reynolds numbers which is comparable with the results obtained in Ref. 12 for 2D cavity flow. The algorithm can be used to more efficiently calculate 3D time-harmonic flows like blood flow in abdominal aorta.

Acknowledgments

This work has been funded by the Dutch National Science Foundation, NWO, through the ToKeN2000 Distributed Interactive Medical Exploratory for 3D Medical Images (DIME) project(634.000.024).

References

1. S. Succi, *The Lattice Boltzmann Equation for Fluid Dynamics and Beyond* (New York:Oxford, 2001).
2. R. Benzi, S. Succi, and M. Vergassola, Phys. Rep. **222**, 145 (1992).

3. Sh. Chen and G. D. Doolen, Annu. Rev. Fluid Mech. **30**, 329 (1998).
4. D. Kandhai, D. Hlushkou, A. G. Hoekstra, P. M. A. Sloot, H. van As and U. Tallarek, Phys. Rev. Lett. **88**, 234501:1-4 (2002).
5. A. M. Artoli, A. G. Hoekstra and P. M. A. Sloot, J. Biom. **39**, 873 (2005).
6. J. A. Cosgrove, J. M. Buick, S. J. Tonge, C. G. Munro, C. A. Greated and D. M. Campbell, J. Phys. A **36**, 2609 (2003).
7. Zh. Guo, Ch. Zheng and T. S. Zhao, J. Sci. Comp. **16**, 569 (2001).
8. B. Chopard and M. Droz, *Cellular Automata Modeling of Physical Systems* (Cambridge University Press, 1998).
9. D. S. Clague, B. D. Kandhai, R. Zhang and P. M. A. Sloot, Phys. Rev. E **61**, 616 (2000).
10. P. Lallemand and L. Luo, Phys Rev. E **61**, 6546 (2000).
11. S. Ansumali and I. V. Karlin, Phys. Rev. E **65**, 056312 (2002).
12. J. Latt and B. Chopard, Math. Comp. Sim. **72**, 165 (2006).
13. J. R. Womersley, Phil. Mag. **46**, 199 (1955).
14. Y. H. Qian, D. d'Humieres and P. Lallemand, Europhys. Lett. **17**, 479 (1992).
15. A. M. Artoli, A. G. Hoekstra and P. M. A. Sloot, Int. J. Mod. Phys. B **17**, 95 (2003).
16. M. Bouzidi, M. Firdaouss and P. Lallemand, Phys. Fluids **13**, 3452 (2001).
17. J. D. Sterling and S. Chen J. Comp. Phys. **123**, 196 (1996).
18. G. Hazi, Phys. Rev. E **67**, 056705 (2003).
19. Y. Shi, T. S. Zhao and Z. L. Guo, Phys. Rev. E **73**, 026704 (2006).
20. L. Axner, A. G. Hoekstra and P. M. A. Sloot, Phys. Rev. E (submitted).